https://doi.org/10.5194/gchron-2021-8
Preprint. Discussion started: 2 March 2021

Age distribution of horizontal fission tracks

Peter Klint Jensen [1], Kirsten Hansen [2]

[1]DTU Civil Engineering, Technical University of Denmark, Kgs. Lyngby, DK–2800, Denmark
[2]Natural History Museum of Denmark, University of Copenhagen, Copenhagen, DK–1350, Denmark

Correspondence to: Peter Klint Jensen (pklje@byg.dtu.dk)

Abstract. Equations for the distribution of age versus length of partially annealed horizontal fission tracks in apatite is presented. Probabilistic least–squares inversion corrects natural track length histograms for observational biases considering the variance of data, modelization, and prior information. The corrected histogram is validated by its variance–covariance matrix. It is considered that horizontal track data can be with or without measurements of angles to the c–axis. In the last case, 3D–histograms are introduced as an alternative to histograms of c–axis projected track lengths. Thermal history modeling of samples is not necessary for track age distribution calculation. In an example the age equations are applied to apatites with pre–depositional (inherited) tracks, to extract the post–depositional track length histogram. Fission tracks generated before deposition in detrital apatite crystals are mixed with post–depositional tracks. This complicates the calculation of the post–sedimentary thermal history as the grains have experienced different thermal histories until deposition. Thereafter the grains share a common thermal history. The extracted post–depositional histogram without inherited tracks may be used for thermal history calculation.

1 Overview of the formation of fission tracks

Fission of U–238 in apatite, sphene, and zircon create tracks in the crystal lattice. Track density is reduced as a function of temperature and time as tracks anneal and shorten due to atom diffusivity (Li et al., 2011; Fleisher et al., 1975; Afra et al., 2011). The ongoing track generation through time and simultaneous annealing is used to derive the thermal history of the sample. Bertagnolli et al. (1983) derived the differential equation describing the track length distribution within a mineral due to annealing through time. The surface density of tracks is also described. Forward calculation examples are given by Bertagnolli et al. (1983). On this basis, Keil et al. (1987) developed an inversion procedure, where the temperature history is derived from either the length distribution of tracks within the crystal or from the length distribution of projected tracks intersecting the surface. The calculation procedure is direct and without the use of a Monte Carlo type optimization. The time of track generation can be derived from the observed track length distribution independent of any annealing law (Keil et al., 1987):

$$\tau(\lambda_0) = \frac{1}{\varepsilon}\int_1^{\lambda_0} n(\lambda)d\lambda\,, \tag{1}$$

where λ_0 is the present track normalized length, ε is the fission–track production rate, $n(\lambda)$ is the measured number of fission tracks of length λ produced per volume. The temperature history is derived from the distribution of projected tracks together

https://doi.org/10.5194/gchron-2021-8
Preprint. Discussion started: 2 March 2021

with an annealing model. Keil et al. (1987) showed, by a synthetic example for projected tracks, that the thermal history can be calculated numerically stepwise backward in time starting with the present temperature. The large uncertainties of projection of tracks mean that the approach by Keil et al. (1987) is dubious. The selection of horizontal, confined tracks are recommended instead (Laslett et al., 1984), that is "tracks identified by the constancy of focus over their entire length and strong reflection in incident illumination" (Gleadow et al., 1986b; Gleadow et al., 2019). The model by Keil et al. (1987) does not include blurring of track length histograms caused by the initial distribution of fission fragment energy (Jungerman and Wright, 1949), annealing and etching anisotropy, mineral composition, the uncertainty of measurement (Ketcham, 2003), and track selection biases Jensen et al. (1992). Proportionality of the number of tracks in a track length histogram column and time assumed by Keil et al. (1987) is disturbed by the blurring. Jensen et al. (1992; 1993) extended Eq. (1) to confined horizontal tracks instead of projected tracks. Belton and Raab (2010) also used a backward cumulative method to estimate the track ages.

Three major biases appear to be important when deriving the equation for track age: 1) Surface track density bias reflecting the likelihood of a track to be exposed to etching on the surface. We use an exponential approximation to surface track density versus mean track length for induced tracks annealed in the laboratory (Green, 1988). 2) Track length bias due to the likelihood of a track being exposed to etching through fractures and tracks cutting the etched surface. We assume it to be proportional to the track length. 3) Selection bias due to the likelihood of an etched track being accepted as horizontal. We assume that tracks within a given angle from the horizontal are counted. The alternative that all tracks in focus are accepted is discussed in Appendix C. Besides biases, there is a range of effects contributing to large observational deviations of track lengths as has been documented in interlaboratory comparisons (Ketcham et al., 2009). The effects are caused by personal etching and observational practice, and sampling statistics. Variation of the number of tracks in a given length interval is dependent on the spontaneous character of fission. The disordering of the unique relationship between track length and time caused by various biases and variances is essentially restored by deconvolution of natural track length histograms (Jensen et al., 1992). Deconvolution is performed by mathematically simulated annealing (Kirkpatrick et al., 1983) and with the use of filters based on annealing of induced tracks in the laboratory. Jensen et al. (1992; 1993) and Jensen and Hansen (2018) used that the track ages can be derived separately from the thermal history as shown by Keil et al. (1987). The columns of the deconvolved track length histogram are then converted to equivalent time intervals. The track ages are obtained by backward cumulation from long tracks toward short tracks. The deconvolution procedure described in Jensen et al. (1992) is for measurements where the c–axis angle is not measured. When they are available it is the practice to project the tracks on the crystal c–axis following the procedure described by Donelick et al. (1999). As an alternative, the inversion method presented here uses 3D–histograms. Age–track length relations are given explicitly in contrast to the indirectly embedded relations in the computer programes by Green et al. (1989), Lutz and Omar (1991), Ketcham (2005), and Gallagher (2012). Our age calculations are calibrated without sample temperature history modeling. The inversion procedure presented here is based on least–squares probabilistic inverse theory (Tarantola, 2005). The method is computational fast.

https://doi.org/10.5194/gchron-2021-8
Preprint. Discussion started: 2 March 2021

2 Equation for the age distribution

Consider a mineral as apatite and a time interval Δt^i in which randomly oriented fission tracks are generated with the initial track length L_o. The number of tracks per unit volume generated in the time interval is proportional to the fission decay frequency λ_f, the uranium U–238 concentration c, and the length of the time interval Δt^i:

$$n^i = \lambda_f c \Delta t^i \text{ for } i = 1 \dots N. \quad (2)$$

N is the number of time intervals. The exponential decay of U–238 nuclei is ignored, to begin with. A track is generated for each fission; therefore, n^i is also the number of initially randomly oriented tracks per unit volume. The track length histogram of the randomly oriented tracks per unit volume generated in a single time interval Δt^i is initially

$$\boldsymbol{n}^i = (n_1^i \dots n_j^i \dots n_M^i)^T. \quad (3)$$

Vectors are bold and the transpose ^{T} transforms rows into columns. M is the number of track length bins. The tracks are gradually annealed from the initial length by temperature and time leading to shorter tracks with the mean track length L^i (Fig. 1). The tracks generated in the time interval Δt^i are after partial annealing distributed into various track length columns. At present, after partial annealing, the track length histogram is

$$\boldsymbol{\nu}^i = (\nu_1^i \dots \nu_j^i \dots \nu_M^i)^T. \quad (4)$$

For the tracks that are not annealed below the detection limit the number of tracks per unit volume ν^i (not bold) is equal to the number of fissions in the time interval that is

$$\nu^i = \sum_{j=1}^{M} \nu_j^i = n^i = \lambda_f c \Delta t^i. \quad (5)$$

The surface track density is initially σ_0^i and at present σ^i, Fig. 1.

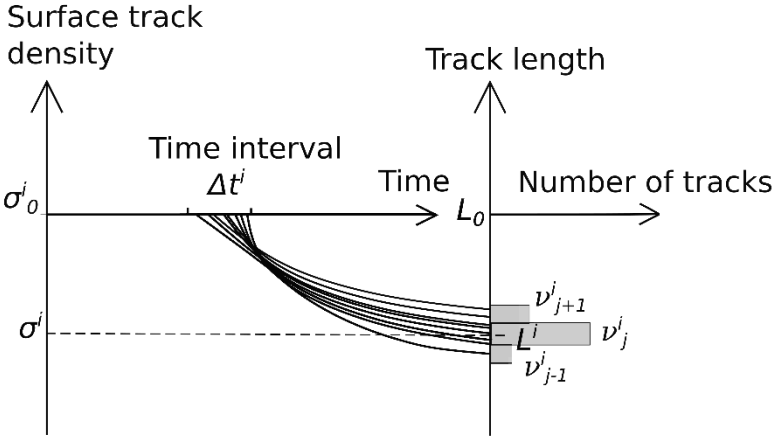

https://doi.org/10.5194/gchron-2021-8
Preprint. Discussion started: 2 March 2021

Figure 1: In the time interval Δt^i, several tracks are spontaneously generated with the initial track length L_0 and surface density σ_0^i. During anisotropic annealing over time, the initial length is reduced along the curved path and spread around the present mean length L^i. Tracks from neighbor time intervals are similarly spread and consequently mixed with tracks from the time interval Δt^i.

A fraction of the randomly oriented tracks $\boldsymbol{v}^i$ cut other tracks connected to the surface providing paths for etchants making them observable in the light microscope. The near–horizontal tracks are selected for length measurements. The track length histogram of the observed near–horizontal tracks generated in the time interval Δt^i is

$$\boldsymbol{h}^i = (h_1^i \dots h_j^i \dots h_M^i)^T. \tag{6}$$

$\boldsymbol{h}^i$ is expected to be linearly dependent on the randomly orientated unexposed tracks $\boldsymbol{v}^i$ which means that the histogram $\boldsymbol{h}^i$ is derived by multiplying the histogram $\boldsymbol{v}^i$ by a set of constants Kk_1^i, .., Kk_M^i:

$$\boldsymbol{h}^i = K(k_1^i v_1^i \dots k_j^i v_j^i \dots k_M^i v_M^i)^T , \tag{7}$$

where K is a proportionality constant. Equation (7) relates the partly annealed randomly oriented unetched tracks to the observed horizontal tracks. The j'th elements of $\boldsymbol{h}^i$ is

$$h_j^i = Kk_j^i v_j^i . \tag{8}$$

The number of observable tracks generated in the time interval Δt^i is

$$h^i = \sum_{j=1}^{M} h_j^i = K \sum_{j=1}^{M} k_j^i v_j^i . \tag{9}$$

It is expected that long tracks are more likely to be etched and observed than short tracks when using the angle selection criteria (Ketcham, 2019). This means that the proportionality constants

$$k_j^i = \frac{L_j^i}{L_0}, \tag{10}$$

where L_j^i is the track length of the partially annealed track. The relation between the randomly oriented tracks to the number of observable tracks is then

$$h^i = \frac{K}{L_0} \sum_{j=1}^{M} (L_j^i v_j^i) . \tag{11}$$

Equation (8) and Eq. (10) lead to:

$$\frac{L_0}{KL_j^i} h_j^i = v_j^i. \tag{12}$$

Summation on both sides of the equation leads to

$$\frac{L_0}{K} \sum_{j=1}^{M} \frac{h_j^i}{L_j^i} = \sum_{j=1}^{M} v_j^i = v^i = n^i = \lambda_f c \Delta t^i, \tag{13}$$

which means that

$$\Delta t^i = \frac{L_0}{K \lambda_f c} \sum_{j=1}^{M} \frac{h_j^i}{L_j^i}. \tag{14}$$

https://doi.org/10.5194/gchron-2021-8
Preprint. Discussion started: 2 March 2021

It is expected that the shape and mean track length of the histogram $\boldsymbol{h}^i$ of observable tracks with origin in the time interval Δt^i can be reproduced in a laboratory annealing experiment:

$$\boldsymbol{h}^i = \hbar^i \boldsymbol{g}^i, \tag{15}$$

where $\hbar^i$ is a proportionality constant. $\boldsymbol{g}^i$ is a track length distribution histogram derived from annealing in the laboratory, or an interpolation thereof:

$$\boldsymbol{g}^i = (g_1^i, g_2^i, \ldots, g_j^i, \ldots g_M^i)^T. \tag{16}$$

$\boldsymbol{g}^i$ and $\boldsymbol{h}^i$ has identical mean track lengths.

$$h^i = \sum_{j=1}^{M} \boldsymbol{h}^i = \sum_{j=1}^{M} \hbar^i g_j^i = \hbar^i \sum_{j=1}^{M} g_j^i = \hbar^i, \tag{17}$$

because $\boldsymbol{g}^i$ is normalized for all i:

$$\sum_{j=1}^{M} g_j^i = 1 \tag{18}$$

The natural observed histogram is the sum over all the histograms $\boldsymbol{h}^i$, each of which linked to time interval i:

$$\boldsymbol{d} = \sum_{i=1}^{N} \boldsymbol{h}^i, \tag{19}$$

and with Eq. (15)

$$\boldsymbol{d} = \sum_{i=1}^{N} \hbar^i \boldsymbol{g}^i, \tag{20}$$

Therefore, a natural fission–track histogram $\boldsymbol{d}$ can be approximated by a weighted sum of interpolated laboratory track length histograms (Fig. 2 and Fig. A1 in Appendix A).

https://doi.org/10.5194/gchron-2021-8
Preprint. Discussion started: 2 March 2021

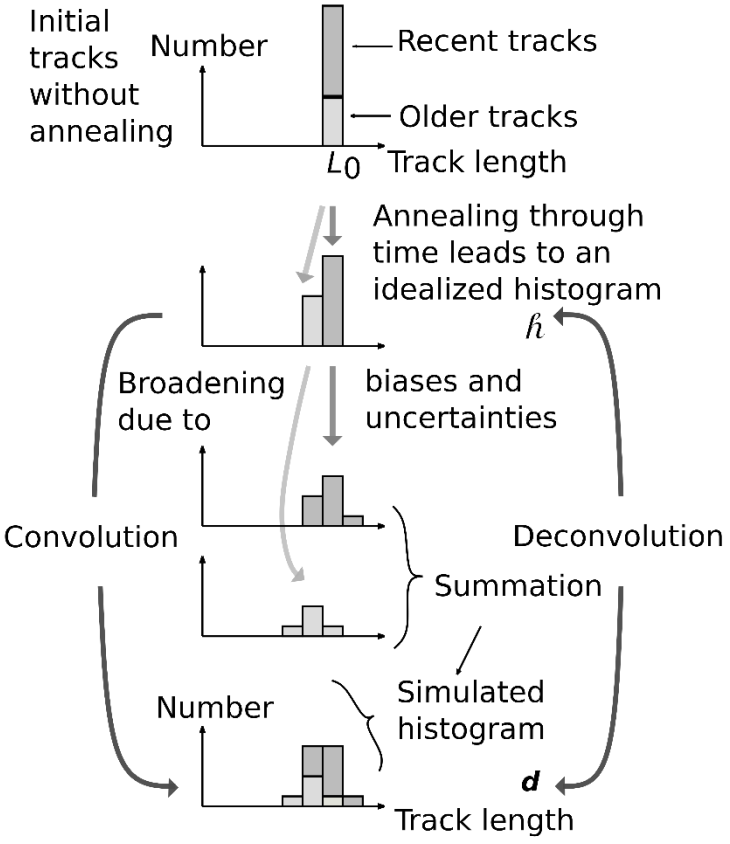

Figure 2. All randomly oriented tracks start with the length L_0 and then annealed by time and temperature. At present the track length histogram is $\tilde{\boldsymbol{\hbar}}$, an idealized histogram without track length broadening effects. The most recent tracks appear in the rightmost column of $\tilde{\boldsymbol{\hbar}}$. This histogram is broadened by convolution to mimic the histogram $\boldsymbol{d}$ resembling a measured histogram. The broadening is caused by 1) tracks initially generated with a distribution of lengths, 2) anisotropic annealing, 3) anisotropic etching, and 4) uncertainties of measurement of track lengths. The convolution itself may be regarded as a summation of the broadening of separate columns of $\tilde{\boldsymbol{\hbar}}$. Deconvolution removes the broadening of $\boldsymbol{d}$.

$\boldsymbol{g}^i$ is a filter transforming the weights $\hbar^i$ into the natural histogram $\boldsymbol{d}$:

$$\boldsymbol{d} = \mathbf{G}\boldsymbol{\hbar}, \tag{21}$$

or

https://doi.org/10.5194/gchron-2021-8
Preprint. Discussion started: 2 March 2021

$$\begin{bmatrix} d^1 \\ d^2 \\ \vdots \\ d^M \end{bmatrix} = \begin{bmatrix} g_1^1 & g_1^2 & \cdots & g_1^N \\ g_2^1 & g_2^2 & \cdots & g_2^N \\ \vdots & \vdots & \cdots & \vdots \\ g_M^1 & g_M^2 & \cdots & g_M^N \end{bmatrix} \cdot \begin{bmatrix} \hbar^1 \\ \hbar^2 \\ \vdots \\ \hbar^N \end{bmatrix}, \tag{22}$$

Each column of the matrix $\mathbf{G}$ is a filter with increasing mean track length from column 1 to N. Solving Eq. (21) for $\boldsymbol{\hbar}$ (the model) is named deconvolution. The equation does not take data variance into account. Therefore, a probabilistic inverse method is used (Tarantola, 2005) assuming Gaussian distributions of variance–covariance of data, prior information, and modelization. The solution (the model) is named the posterior $\tilde{\boldsymbol{\hbar}}$ (Tarantola, 2005):

$$\tilde{\boldsymbol{\hbar}} = \boldsymbol{\hbar}_{prior} + (\mathbf{G}^T \mathbf{C}_D^{-1} \mathbf{G} + \mathbf{C}_H^{-1})^{-1} \mathbf{G}^T \mathbf{C}_D^{-1} (\boldsymbol{d}_{obs} - \mathbf{G}\boldsymbol{\hbar}_{prior}). \tag{23}$$

Prior information $\boldsymbol{\hbar}_{prior}$ is derived from other independent information or, if not available, simply homogeneous with the elements equal to the mean value of the number of measured tracks. $\mathbf{C}_D$ is the variance–covariance matrix of the natural observed data $\boldsymbol{d}_{obs}$. The measurements of a given number of track lengths are statistically considered as several possible outcomes of a trial greater than two. The multinomial statistical distribution is therefore used to describe variance–covariance. The diagonal elements of $\mathbf{C}_D$ are the variances of the observed number of tracks for each length interval.:

$$\mathbf{C}_D(j,j) = DP^j(1-j) \qquad \text{for } j = 1 \ldots M, \tag{24}$$

where $P^i = d_{obs}^i / D$ is the probability of the observed data d^i. D is the number of measured natural tracks. The off–diagonal elements are the covariances

$$\mathbf{C}_D(l,j) = -DP^l P^j \qquad \text{for } l \neq j. \tag{25}$$

Modelization variance caused by the variance of $\mathbf{G}$, Eq. (21), is calculated by forward modelling using Eq. (21) and added to $\mathbf{C}_D$ (Tarantola, 2005). This variance is calculated by random Gaussian realizations of the filters assuming the standard deviations to be $\sqrt{\boldsymbol{g}^i}$. The variance–covariance matrix $\mathbf{C}_H$ for the prior is calculated similarly to $\mathbf{C}_D$. When the influence of prior information is unwanted large variance values are given as diagonal elements of the matrix $\boldsymbol{C}_H$. The variance–covariance of the posterior is calculated following Tarantola (2005):

$$\widetilde{\mathbf{C}_H} = (\mathbf{G}^T \mathbf{C}_D^{-1} \mathbf{G} + \mathbf{C}_H^{-1})^{-1}. \tag{26}$$

An approximation to the observed data $\boldsymbol{d}_{obs}$ is calculated forwardly using the posterior:

$$\widetilde{\boldsymbol{d}_{obs}} = \mathbf{G}\tilde{\boldsymbol{\hbar}}. \tag{27}$$

The deconvolved histogram $\tilde{\boldsymbol{\hbar}}$ is essential for track age calculation as discussed below.

The density σ^i of induced tracks, generated in the time interval Δt^i, intersecting a polished surface plane of the mineral is related to the mean track length (Green et al., 1986). It is here approximated by a logarithmic expression (Appendix B):

$$\frac{\sigma^i}{\sigma_0^i} = \left[1 + \frac{1}{b} \ln\left(\frac{L^i}{L_0}\right)\right], \tag{28}$$

https://doi.org/10.5194/gchron-2021-8
Preprint. Discussion started: 2 March 2021

where $\frac{\sigma^i}{\sigma_0^i}$ is the reduced surface track density, $\frac{L^i}{L_0}$ is the reduced mean track length, and b is a calibration constant dependent on the mineral composition. Natural tracks generated in the time interval Δt^i and with a present mean track length L^i is expected to have the same reduced surface track density as laboratory annealed tracks with the same reduced mean track length. Equation (28) is therefore also valid for the natural tracks. The initial surface track density σ_0^i generated in the time interval Δt^i is expected to be proportional to the initial mean track length and time

$$\sigma_0^i = ½\xi\lambda_f c L_0 \, \Delta t^i, \tag{29}$$

where ξ is a calibration constant. Combining Eq. (28) and Eq. (29) leads to the surface track density assigned to the time interval Δt^i:

$$\sigma^i = ½\xi\lambda_f c \mathcal{L}^i \Delta t^i, \tag{30}$$

where

$$\mathcal{L}^i = [\, 1 + \frac{1}{b} \ln\left(\frac{L^i}{L_0}\right)] L_0 \, . \tag{31}$$

The value of $\mathcal{L}^i$, having the unit of length, is less than the mean track length L^i and is considered as a correction to the mean track length L^i. The natural surface track density σ_s is composed of contributions from all the time intervals

$$\sigma_s = \sum_{i=1}^{N} \sigma^i \, , \tag{32}$$

Inserting the right side of Eq. (30) instead of σ^i in Eq. (32) leads to

$$\sigma_s = ½\xi\lambda_f c \sum_{i=1}^{N} (\mathcal{L}^i \Delta t^i). \tag{33}$$

Remembering that $h^i = \hbar^i$, Eq.(17), and that the result of the inversion $\tilde{\hbar}^i$ is an approximation to h^i we get together with Eq.(14)

$$\sigma_s = \frac{\xi L_0}{2K} \sum_{i=1}^{N} (\mathcal{L}^i \sum_{j=1}^{M} (\frac{\tilde{\hbar}_j^i}{L_j^i})). \tag{34}$$

Inserting Eq. (14) for Δt^i into Eq. (30) leads to

$$\sigma^i = ½\xi\lambda_f c \mathcal{L}^i \Delta t^i = \frac{\xi L_0}{2K} \mathcal{L}^i \sum_{j=1}^{M} (\frac{\tilde{\hbar}_j^i}{L_j^i}). \tag{35}$$

The ratio between σ^i and σ_s is

$$\sigma^i = \sigma_s \frac{\mathcal{L}^i \sum_{j=1}^{M} (\frac{\tilde{\hbar}_j^i}{L_j^i})}{\sum_{i=1}^{N} \left(\mathcal{L}^i \sum_{j=1}^{M} (\frac{\tilde{\hbar}_j^i}{L_j^i}) \right)} \, . \tag{36}$$

This equation is used to calculate the surface track density caused by tracks generated in the time interval Δt^i given the surface track density σ_s and the corrected histogram $\tilde{\boldsymbol{\hbar}}$. An expression for the time interval Δt^i is obtained combining Eq. (30) and Eq. (36), and isolating the time interval on the left side:

https://doi.org/10.5194/gchron-2021-8
Preprint. Discussion started: 2 March 2021

$$\Delta t^i = \frac{2\sigma_s}{\xi\lambda_f c}\frac{\Sigma_{j=1}^{M}(\frac{\tilde{\hbar}_j^i}{L_j^i})}{\Sigma_{i=1}^{N}\left(\mathcal{L}^i\Sigma_{j=1}^{M}(\frac{\tilde{\hbar}_j^i}{L_j^i})\right)}. \quad (37)$$

The formation time (age) for the oldest track t_p in each column p of the histogram $\tilde{\boldsymbol{\hbar}}$ is the cumulation of the time intervals Δt^i corresponding to the column p and younger columns.

$$t_p = \sum_{i=p}^{N}\Delta t^i. \quad (38)$$

That is

$$t_p = \frac{2\sigma_s}{\xi\lambda_f c}\frac{\Sigma_{i=p}^{N}\Sigma_{j=1}^{M}(\frac{\tilde{\hbar}_j^i}{L_j^i})}{\Sigma_{i=1}^{N}\left(\mathcal{L}^i\Sigma_{j=1}^{M}(\frac{\tilde{\hbar}_j^i}{L_j^i})\right)}. \quad (39)$$

The unit of $\tilde{\hbar}_j^i$ is number/m^3 but since it appears both in the nominator and denominator $\tilde{\hbar}_j^i$ can as well be considered dimensionless. Therefore the volume need not be measured. The decreasing uranium concentration through time is considered by introducing the logarithm in Eq. (39).

$$t_p = \frac{1}{\lambda_D} ln\,(\,1 + \frac{2\sigma_s\lambda_D}{\xi\lambda_f c}\frac{\Sigma_{i=p}^{N}\Sigma_{j=1}^{M}\left(\frac{\tilde{\hbar}_j^i}{L_j^i}\right)}{\Sigma_{i=1}^{N}\left(\mathcal{L}^i\Sigma_{j=1}^{M}\left(\frac{\tilde{\hbar}_j^i}{L_j^i}\right)\right)}), \quad (40)$$

where λ_D is the total decay constant. The corresponding surface track density is

$$\sigma_p = \sum_{i=p}^{N}\sigma^i, \quad (41)$$

and using Eq. (36)

$$\sigma_p = \sigma_s\frac{\Sigma_{i=p}^{N}\mathcal{L}^i\Sigma_{j=1}^{M}(\frac{\tilde{\hbar}_j^i}{L_j^i})}{\Sigma_{i=1}^{N}\left(\mathcal{L}^i\Sigma_{j=1}^{M}(\frac{\tilde{\hbar}_j^i}{L_j^i})\right)}. \quad (42)$$

Eq(39) and Eq. (42) are valid for tracks selected within a given angle from the horizontal. Equations for the case when tracks are selected following the requirement that both ends are in focus at the same time are given in Appendix C.

Inversion following Eq. (23) applies both for data measured in the old–fashioned way where track angle to the c–axis is not measured as well as for new measurements which include the angle, Appendix D.

3 Variance of ages

The oldest age $t_p$of tracks in column p given by Eq. (39) and repeated here:

https://doi.org/10.5194/gchron-2021-8
Preprint. Discussion started: 2 March 2021

$$t_p = \frac{2\sigma_s}{\xi\lambda_f c} \frac{\sum_{i=p}^{N}\sum_{j=1}^{M}(\frac{\tilde{\hbar}_j^i}{L_j^i})}{\sum_{i=1}^{N}\left(\mathcal{L}^i\sum_{j=1}^{M}(\frac{\tilde{\hbar}_j^i}{L_j^i})\right)} \quad (43)$$

and approximately

$$t_p \approx \frac{2\sigma_s}{\xi\lambda_f c} \frac{\sum_{i=p}^{N}(\frac{\hbar^i}{L^i})}{\sum_{i=1}^{N}\left(\mathcal{L}^i\frac{\hbar^i}{L^i}\right)} \quad (44)$$

The variance of t_p is derived through the variance of the three parts f_1, f_2, and f_3 of the equation:

$$f_1 = \frac{2\sigma_s}{\xi\lambda_f c}, \quad (45)$$

$$f_2(p) = \sum_{i=p}^{N}(\frac{\hbar^i}{L^i}), \quad (46)$$

$$f_3 = \sum_{i=1}^{N}\left(\mathcal{L}^i\frac{\hbar^i}{L^i}\right). \quad (47)$$

The age of the oldest track in column p is then

$$t_p \approx f_1\frac{f_2(p)}{f_3}. \quad (48)$$

The variance of each part is calculated using standard textbook statistics. The variance of f_1 is

$$Var(f_1) = \left(\frac{\partial f_1}{\partial\sigma_s}\right)^2 \cdot Var(\sigma_s) + (\frac{\partial f_1}{\partial\xi})^2 \cdot Var(\xi) + (\frac{\partial f_1}{\partial\lambda_f})^2 \cdot Var(\lambda_f) + (\frac{\partial f_1}{\partial c})^2 \cdot Var(c) \quad (49)$$

The second part f_2 is a cumulation of correlated histogram columns $\frac{\hbar^i}{L^i}$. The variance of f_2 therefore includes the covariance:

$$Var(f_2(p)) = \sum_{i=p}^{N} Var(\frac{\hbar^i}{L^i}) + 2\sum_{p\le i<j\le M} Cov(\frac{\hbar^i}{L^i}, \frac{\hbar^i}{L^i}) \xrightarrow{yields} \quad (50)$$

$$Var(f_2(p)) = \sum_{i=p}^{N} \frac{1}{L^{i2}} Var(\hbar^i) + 2\sum_{p\le i<l\le N} \frac{1}{L^i L^l} Cov(\hbar^i, \hbar^l) \quad (51)$$

The variance of f_3 is

$$Var(f_3) = \sum_{i=1}^{N} Var(\mathcal{L}^i\frac{h^i}{L^i}) = \sum_{i=1}^{N} \mathcal{L}^{i2} Var\left(\frac{h^i}{L^i}\right) + \left(\frac{h^i}{L^i}\right)^2 Var(\mathcal{L}^i) \quad (52)$$

where

$$Var(\mathcal{L}^i) = (L_0 \ln(\frac{L^i}{L_0}))^2 \frac{1}{b^4} Var(b). \quad (53)$$

The equation for the age, Eq. (48) repeated, is written in terms of the three parts

$$t_p = f_1\frac{f_2(p)}{f_3}. \quad (54)$$

The variance of t_p is then

$$Var(t_p) = (f_1\frac{f_2(p)}{f_3})^2 Var(f_3) + (\frac{f_1}{f_3})^2 Var(f_2(p)) + (\frac{f_2(p)}{f_3})^2 Var(f_1). \quad (55)$$

https://doi.org/10.5194/gchron-2021-8
Preprint. Discussion started: 2 March 2021

4 Inherited tracks

The deconvolution technique can be used to extract the post–depositional part of track length histograms with inherited tracks. This is illustrated in Fig. 3 by an idealized (no broadening) model for track annealing and observation. Grains from two source areas are considered. There are more tracks in the post–depositional columns of Grain 2 than in Grain 1 because it is assumed that the uranium content of Grain 2 is twice that of Grain 1. The two post–depositional columns of Grain 1 and 2 represent the same two time intervals. For both Grain 1 and 2, there is one column where pre–and post–depositional tracks are mixed. This column and the pre–depositional columns of both grain types do not necessarily represent the same time intervals because their different thermal histories create individual track length distributions (histograms). The pre–depositional tracks of Grain 1 compared with those of Grain 2 have experienced different thermal histories and therefore different degree of annealing. Post–depositional tracks are ordered with decreasing length as a function of time in contrast to the pre–depositional tracks which may be disordered. Fig. 3C sums Grain 1 and 2 histograms. It is observed that the post–depositional time intervals for the bulk histogram are identical to those for the two separate grain types. The age equation, Equation (40), is valid for post–depositional tracks but not for mixed or pre–depositional tracks.

https://doi.org/10.5194/gchron-2021-8
Preprint. Discussion started: 2 March 2021

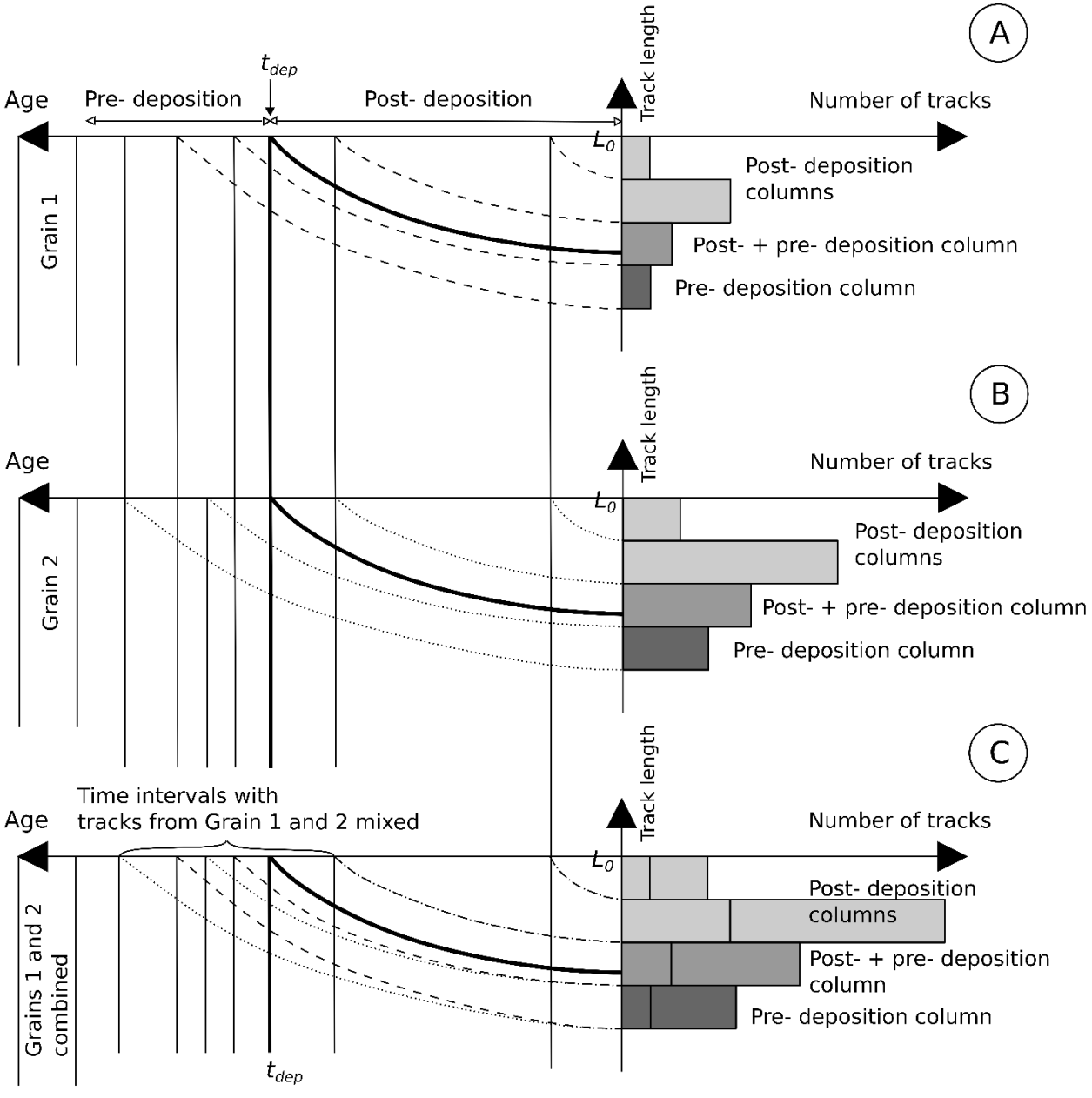

https://doi.org/10.5194/gchron-2021-8
Preprint. Discussion started: 2 March 2021

Figure 3: Sketch for the accumulation of tracks in histogram columns. All tracks start with the length L_0. Some tracks are generated before deposition and some after. The actual track lengths are reduced as a function of time; (A) Grain 1; (B) Grain 2 which has experienced a different pre–depositional thermal history; (C) Histogram for the bulk of Grain 1 and 2.

The post–depositional part of the deconvolved histogram $\tilde{\boldsymbol{h}}$ are the columns having track ages t_p less than the deposition age t_{dep}:

$$t_p \leq t_{dep}\ , \tag{56}$$

where p is the column number. Together with Eq. (40), we obtain

$$\frac{1}{\lambda_D} ln\ (\ 1 + \frac{2\sigma_s \lambda_D}{\xi \lambda_f c} \frac{\Sigma_{i=p}^{N} \Sigma_{j=1}^{M} \left(\frac{\tilde{h}_j^i}{L_j^i}\right)}{\Sigma_{i=1}^{N} \left(\mathcal{L}^i \Sigma_{j=1}^{M} \left(\frac{\tilde{h}_j^i}{L_j^i}\right)\right)}\ ) \leq \quad t_{dep}. \tag{57}$$

The values of p satisfying the inequality identifies the post–sedimentary columns. The smallest number of p identifies the oldest post–sedimentary track. This number is used to calculate the surface track density ρ_{post} linked to the post–depositional histogram by Eq. (42):

$$\sigma_{post} = \sigma_s \frac{\Sigma_{i=post}^{N} \mathcal{L}^i \Sigma_{j=1}^{M} (\frac{\tilde{h}_j^i}{L_j^i})}{\Sigma_{i=1}^{N} \left(\mathcal{L}^i \Sigma_{j=1}^{M} (\frac{\tilde{h}_j^i}{L_j^i})\right)}\ . \tag{58}$$

Summations are performed for all columns representing the post–sedimentary history. Together with the surface track density σ_{post} the post–depositional histogram may be used to calculate the post–depositional thermal history applying the backward modeling procedure described by Jensen et al. (1992). Alternatively, the post–depositional de–convolved histogram can be convolved by forward calculation by Eq. (27) and used by random or guided–random search algorithms (Lutz and Omar, 1991; Willett, 1997; Ketcham, 2005; Gallagher, 1995; 2012).

Identification of post–sedimentary fission–tracks is exemplified by applying apatites from the sample GGU103113 (Jameson Land, East Greenland). The Middle Jurassic sandstone sample (170 Ma) has the apparent fission–track age 245 Ma (Hansen et al., 2001). The measured and the deconvolved track length distributions are shown in Fig. 4a and 4b.

https://doi.org/10.5194/gchron-2021-8
Preprint. Discussion started: 2 March 2021

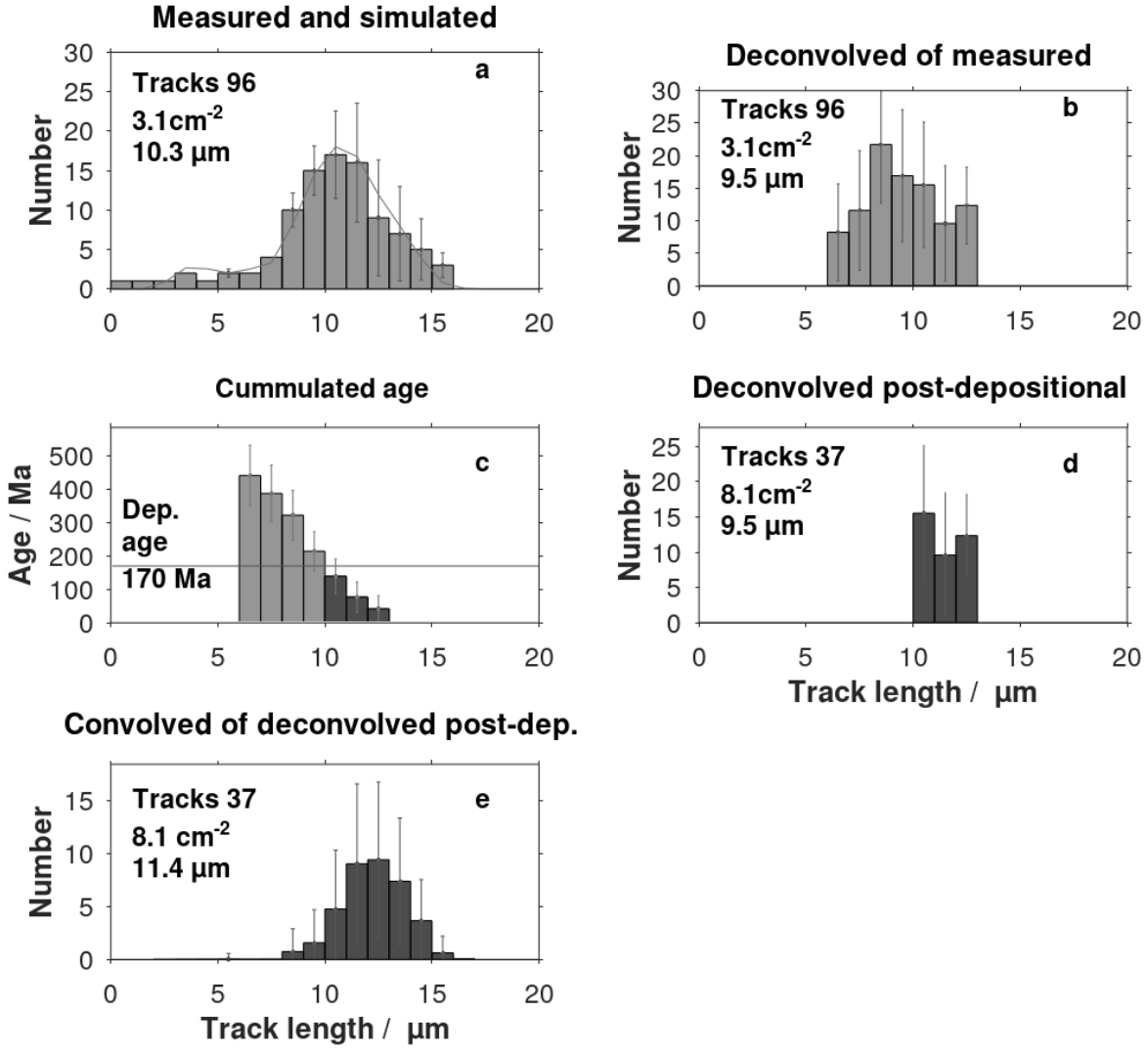

Figure 4: Extraction of the post–sedimentary part of a track length histogram from Jameson Land, East Greenland (Hansen, 1996). The unit of surface track density is cm^{-2}. (a) Measured and simulated (thin line) fission–track length histogram; (b) The histogram after deconvolution using the filters shown in Appendix A; (c) Track ages are calculated by Eq. (40) using the deconvolved histogram. The columns (dark grey) with track ages less than the deposition age (170 Ma) are identified; (d) The post–sedimentary histogram is extracted from the deconvolved histogram based on the identified post–depositional columns. This histogram is the basis for direct calculation of the temperature history (Jensen et al., 1992); (e) The convolved post–sedimentary histogram, resembling a measured histogram, can be used by Monte Carlo type simulation models (Ketcham, 2005; Gallagher, 1995).

The parameter ξ in the age equation, Eq. (40) is adjusted to 0.752 (with b = 0.784) to obtain simulated apparent age equal to the apparent age reported by Hansen et al. (2001). The apparent age is calculated using a track length distribution of an unannealed track length distribution in Eq. (40). The post–depositional columns are identified as being the rightmost columns

https://doi.org/10.5194/gchron-2021-8
Preprint. Discussion started: 2 March 2021

with accumulated ages less than the deposition age, Fig. 4c and Fig. 4d. The deconvolved histogram Fig. 4d can be used to calculate the post–sedimentary thermal history. The histogram in Fig. 4e is the convolution of the histogram in Fig. 4d.

5 Discussion

The equations for accumulated fission–tracks derived here are based on the practice of selecting horizontal tracks for length measurements. We follow the recommendation by Ketcham (2019) who selects all tracks within ±10° from the horizontal. Alternatively, Gleadow et al. (1986b) and Galbraith (2005) select tracks observed in reflected light being within ±10° from the horizontal and with both ends in focus in transmitted light. Fewer long tracks (> 8.5 µm) are then selected relatively to shorter tracks (Appendix C). An alternative set of equations are given in Appendix C for this situation.

Standard deviations of the ages are calculated based on the variance of input data, prior model, and modelization. The calculated deviations are high but they agree with deviations of histograms reported in an interlaboratory comparison (Ketcham et al., 2009). It is required that the laboratory annealed tracks are measured in the same way as the natural tracks. E.g., in the Jameson Land example, the recommendations by Gleadow et al., (1986b) and Gleadow et al., (2019) are used in both cases.

The inversion procedure by Tarantola (2005) requires a prior model being independent of data. As the default, a prior model histogram with an equal number of tracks in the columns is chosen. In some cases, negative track length histogram columns appear as a result of inversion because due to unrealistic data. An improved prior model based on other information is then necessary. The problem can be managed by smoothing of input data and/or of covariance matrices.

When track angles to the c–axis is available it is common practice to calculate the histogram of the c–axis projected tracks. However, detailed information on track density is lost along the accumulation along the projection path. Instead, one can use 3D–track length histograms as described in Appendix D. 3D–histograms do not involve projections and therefore retain both length and angle information. The inversion procedure presented here is valid for both 2D– and 3D–histograms (Appendix D).

6 Conclusions

A new procedure for deriving fission–track ages as a function of track length is suggested. The natural fission–track length histogram is considered as linearly composed of histograms of induced tracks partially annealed in the laboratory. Inversion is performed by a probabilistic inverse theory. The resulting track ages are given as centers of posterior with variance. The equations are valid for old–type measurements where the track angle to the c–axis is not measured as well as for recent data including measurements of the angle to the c–axis. Data with both track lengths and angles are organized in 3D–histograms presented as images. Two types of track length measurements are discussed. If tracks with both ends in focus are selected there

https://doi.org/10.5194/gchron-2021-8
Preprint. Discussion started: 2 March 2021

is a tendency to off–select longer tracks. If all tracks within a given angle are selected this bias disappears. The equations presented here are prepared for both cases. The calculation of track ages does not require the calculation of the sample thermal history. Instead, they are the basis for temperature history calculation. As an example, the deconvolution method presented here is used to identify the post–depositional part of a track length histogram from Jameson Land, Greenland.

Appendix A

The filters used for deconvolution are the columns of matrix **G**, Eq. (22). They are based on measurements of track lengths after annealing in the laboratory (Gleadow et al., 1986a; Green et al., 1986; Barbarand et al., 2003). The histograms of these track lengths are normalized by division with the number of tracks of each histogram. They represent the probability of an induced track to appear in a certain length interval. Interpolated filters are obtained using a mesh of 0.2 μm in both directions (bins and mean track lengths), Fig. A1.

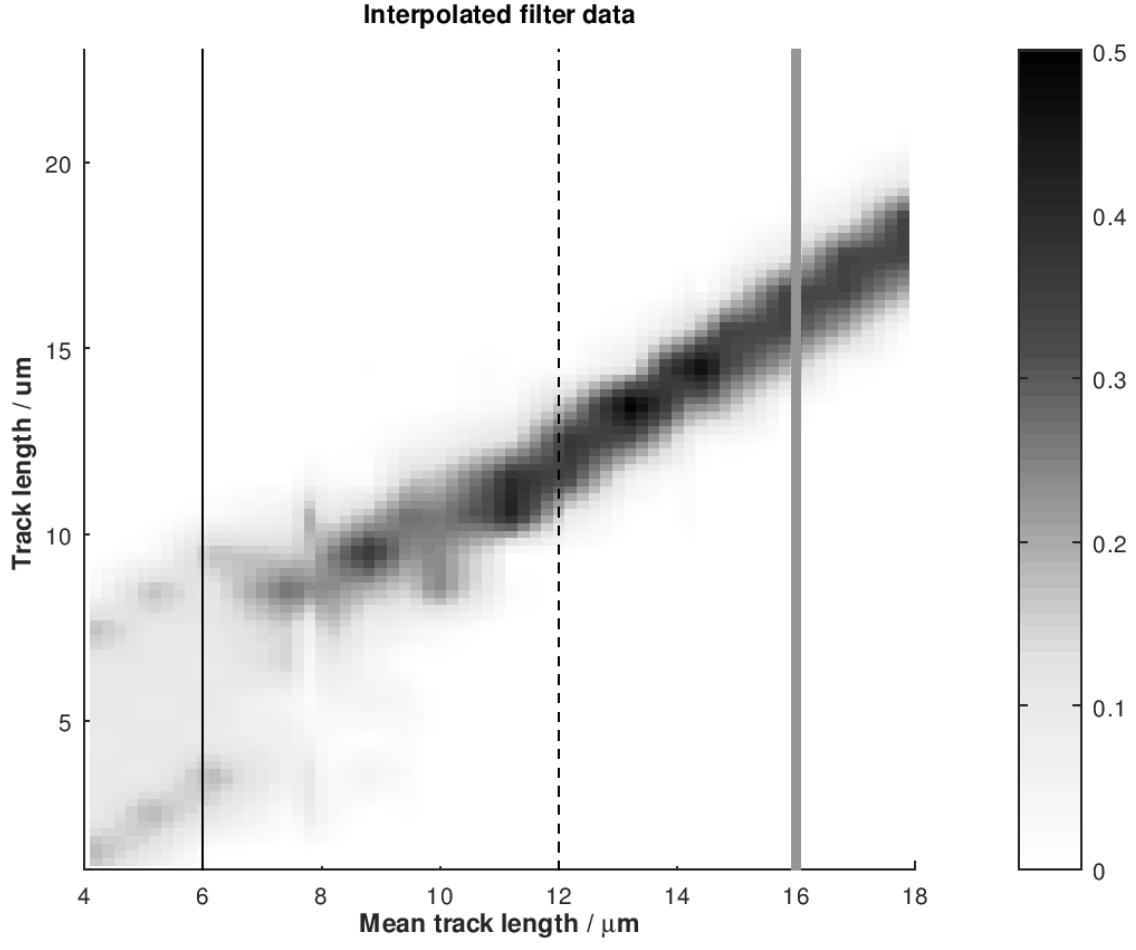

https://doi.org/10.5194/gchron-2021-8
Preprint. Discussion started: 2 March 2021

Figure A1. Interpolation of the filters used for deconvolution. It is based on track annealing in the laboratory (Gleadow et al., 1986a; Green et al., 1986; Barbarand et al., 2003). Three linear intersections are shown in Fig. A2. Grayscale is frequency.

The filters broaden with decreasing mean track length. The columns of the modelization matrix **G** are picked from the interpolation. The number of columns is related to the resolution. Fig. A2 shows three filters extracted from Fig. A1.

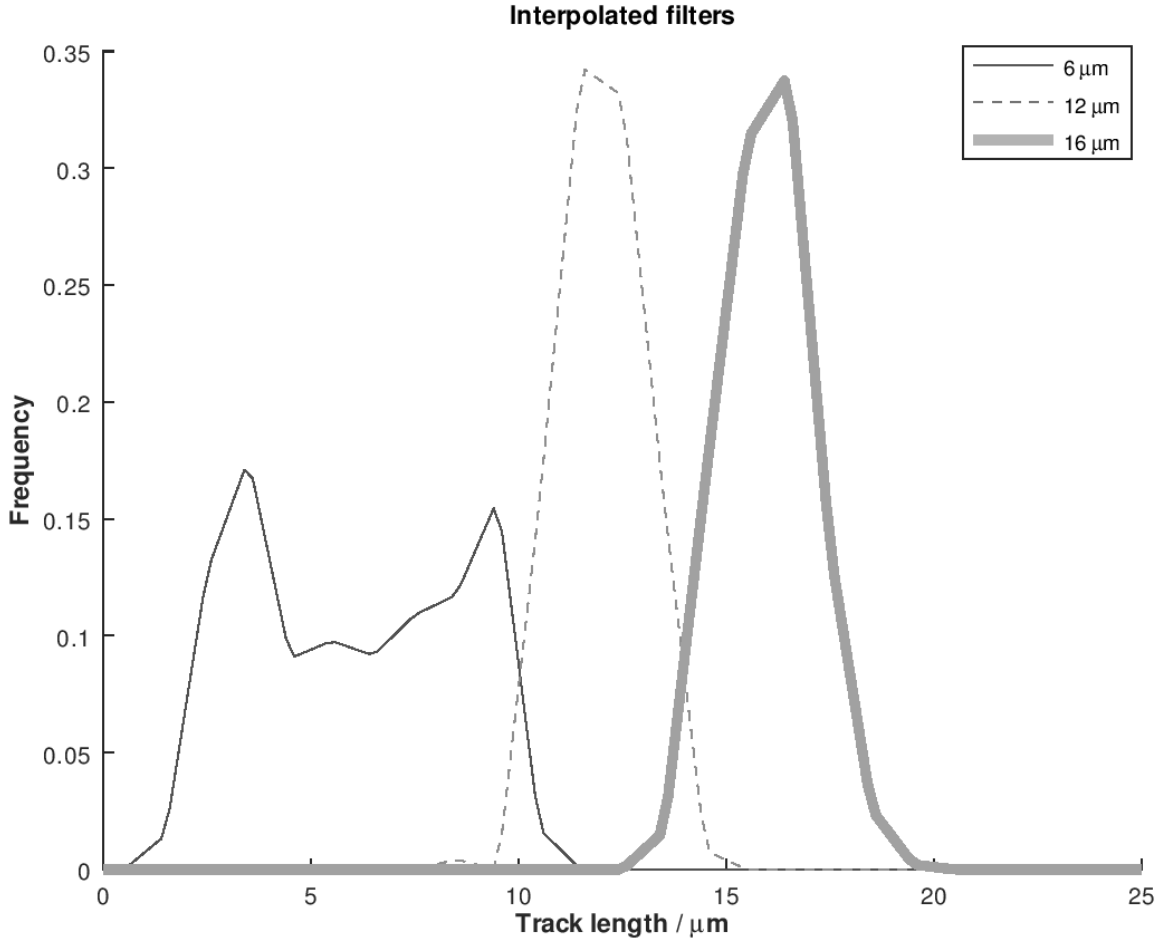

Figure A2: Three interpolated filters with mean track lengths 6, 12, and 15 μm extracted from Fig. A1.

Appendix B

Plots of mean track length versus surface track density for tracks generated by neutron radiation and annealed in the laboratory are given by Green et al. (1986). A logarithmic expression approximates data, Fig. B1:

$$\frac{\sigma^i}{\sigma_0^i} = \left[1 + \frac{1}{b}\ln\left(\frac{L^i}{L_0}\right)\right], \quad \text{(A1)}$$

https://doi.org/10.5194/gchron-2021-8
Preprint. Discussion started: 2 March 2021

where σ^i/σ_0^i is the surface track density of partially annealed tracks relatively that of unannealed tracks. L^i/L_0 is the mean track length of partially annealed tracks relative to the unannealed mean track length. Equation (A1) is used to parameterize the measured data leading to $b = 0.748 \pm 0.048$ for multi–compositional apatite and b = 0.963 for mono–compositional apatite. b determines the curvature of the approximating line in Fig. B1.

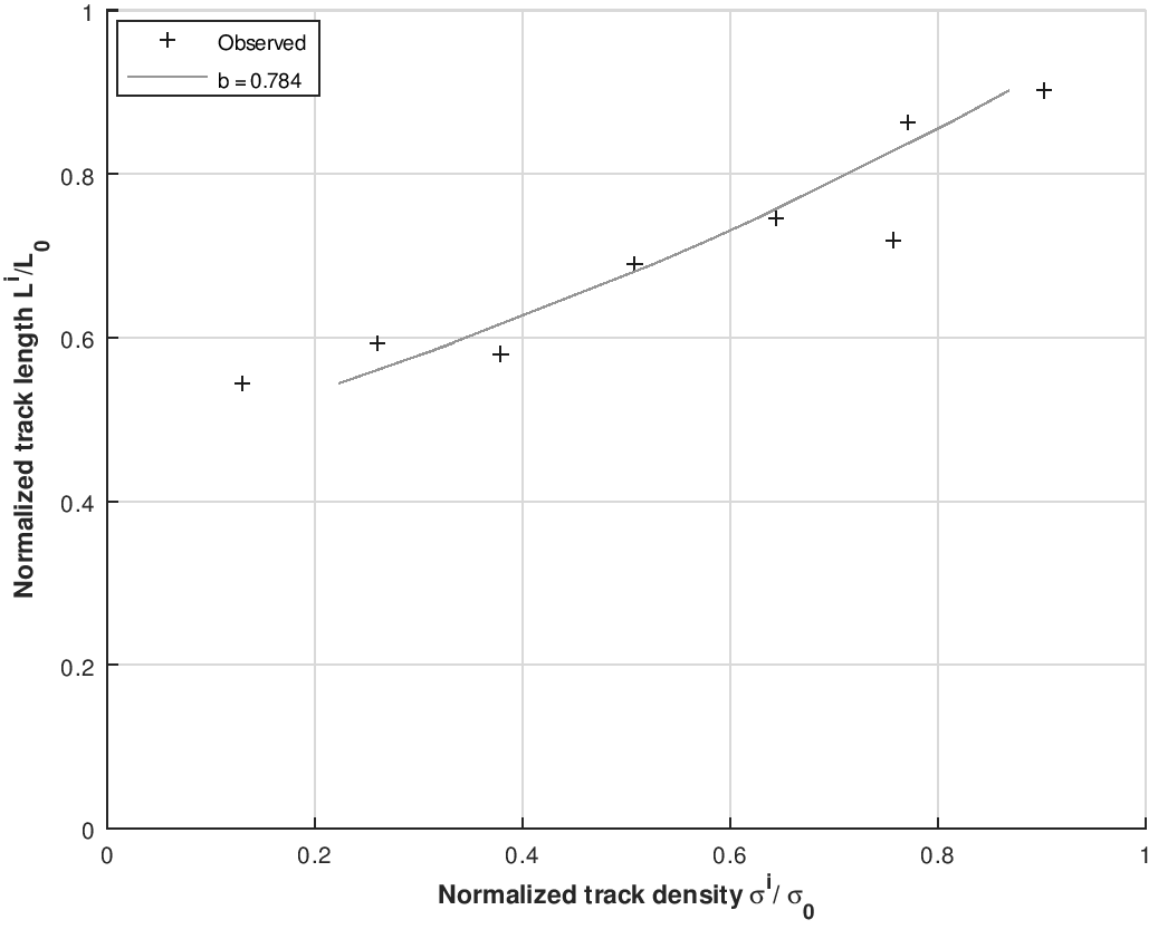

Figure B1: Parameter b characterizes the relation between normalized track length L^i/L_0 and normalized density σ^i/σ_0^i for multi–compositional apatite. Data from Green et al. (1988).

Appendix C

Ketcham (2019) recommends the selection of all etched tracks being within ±10° from the horizontal. It is expected that the likelihood of tracks being etched is proportional to their length. This view has been adopted in the main text of this paper.

https://doi.org/10.5194/gchron-2021-8
Preprint. Discussion started: 2 March 2021

Alternatively to the selection criteria by Ketcham (2019), Gleadow et al (2019) select etched tracks that are within 10°–15° from the horizontal and with both ends in focus at the same time. The two criteria are examined in this appendix.

The axial (vertical) resolution of a light microscope is

$$r_{axial} = 1.4\lambda\eta/NA^2. \quad \text{(C1)}$$

With typical values for wavelength of λ = 550 nm (green light), refraction index of oil η = 1.51, and numerical aperture NA = 1.25, the axial resolution r_{axial} = 0.74 µm. The numerical aperture is a measure of the maximum angle for which the microscope receives light. The criteria by Gleadow et al (2019) imply that a short track, 6 µm long, is accepted for counting if the angle to the horizontal is less than 10°. A long track, 18 µm, has to be within 2.5° to the horizontal to be accepted. The tendency is therefore that long tracks are off–selected from counting. The likelihood of selection is then inverse proportional to the track length for tracks longer than 6 µm. At the same time, the likelihood of a horizontal track being etched is expected to be proportional to its length. These two biases essentially cancel each other (Jensen et al., 1992). With the focus window selection criteria (Gleadow et al., 2019) the set of age equations is then:

$$t_p = \frac{1}{\lambda_D} ln\,(\,1 + \frac{2\sigma_s\lambda_D}{\xi\lambda_{fc}} \frac{\sum_{i=p}^{N} \tilde{n}^i}{\sum_{i=1}^{N}(\mathcal{L}^i\tilde{n}^i)}\,) \quad \text{(C2)}$$

The age of the oldest track is obtained summing all the time intervals:

$$t_{max} \sim \frac{2\sigma_s}{\xi\lambda_{fc}} \frac{\sum_{i=1}^{N} \tilde{n}^i}{\sum_{i=1}^{N}(\mathcal{L}^i\tilde{n}^i)}\,. \quad \text{(C3)}$$

Introducing the mean track length of the inverted histogram $\tilde{\boldsymbol{n}}$:

$$\mathcal{L}_{mean} = \frac{\sum_{i=1}^{N}(\mathcal{L}^i\tilde{n}^i)}{\sum_{i=1}^{N}\tilde{n}^i}\,. \quad \text{(C4)}$$

The age of the oldest observable track is

$$t_{max} = \frac{2\sigma_s}{\xi\lambda_{fc}\mathcal{L}_{mean}}\,, \quad \text{(C5)}$$

equivalent to the derivation by Jensen et al. (1992) when $\mathcal{L}_{mean}$is replaced by the mean track length.

Appendix D

The inversion principle presented in the main text is for 2D–track length histograms ignoring track angles to the c–axis. However, the inversion principle is also applicable to data that includes the angles. The measured data vector $\boldsymbol{d}_{obs}$ in Eq. (22) is then derived from a 3D–histogram (length, angle, and number). The elements of the vector $\boldsymbol{d}_{obs}$ is obtained by sequentially numbering each bin (Tarantola, 2005). An example is shown in Fig. D1 with a synthetic 3D–histogram as data obtained from two annealing experiments.

https://doi.org/10.5194/gchron-2021-8
Preprint. Discussion started: 2 March 2021

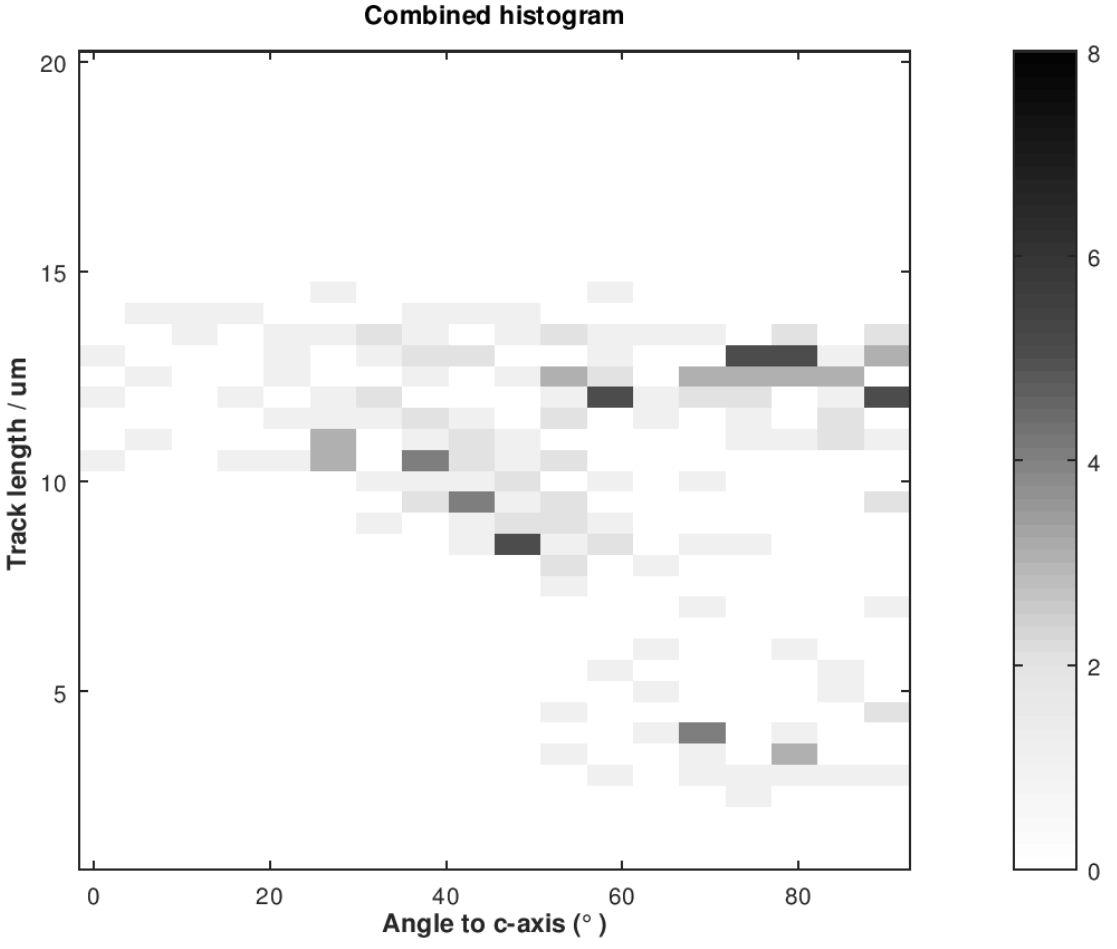

395

Figure D1. 3D–histogram of track lengths versus angles derived by combining two annealing experiments (Barbarand et al., 2003). Grayscale is the number of tracks in each bin.

They are the result of heating to 275ºC and 320ºC respectively (Barbarand et al., 2003). Each bin of the 3D–histogram is 5º
400 times 0.5 µm. The matrix **G**, Eq. (22) consists of twenty 3D–filters interpolated between the six annealing experiments by Barbarand et al. (2003). Each column of **G** is a filter. Two of them are shown in Fig. D2.

https://doi.org/10.5194/gchron-2021-8
Preprint. Discussion started: 2 March 2021

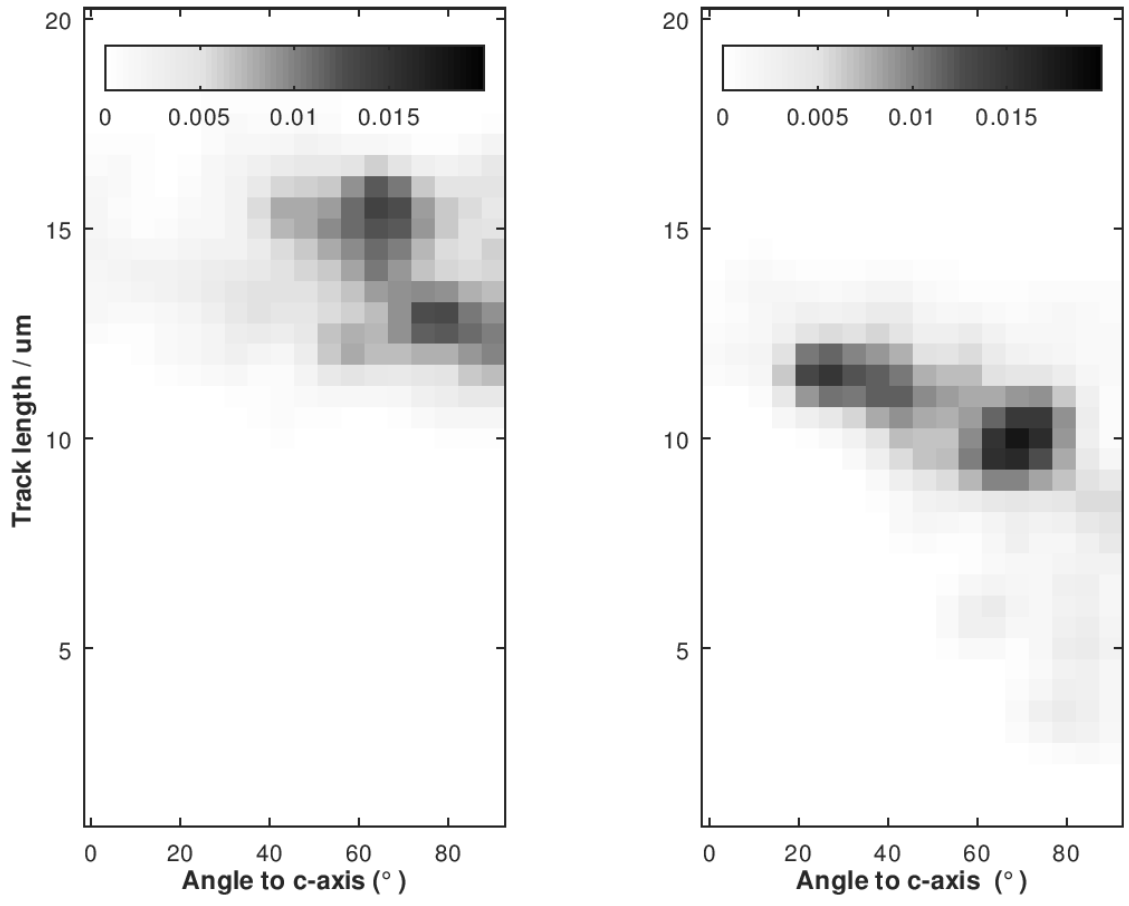

405 **Figure D2: Examples of 3D–filters used for deconvolution. They are based on heating to 275°C and 320°C respectively, Barbarand et al. (2003). Greyscale is frequency.**

The corrected histogram as a result of the inversion using Eq. (22) is shown in Fig. D3.

https://doi.org/10.5194/gchron-2021-8
Preprint. Discussion started: 2 March 2021

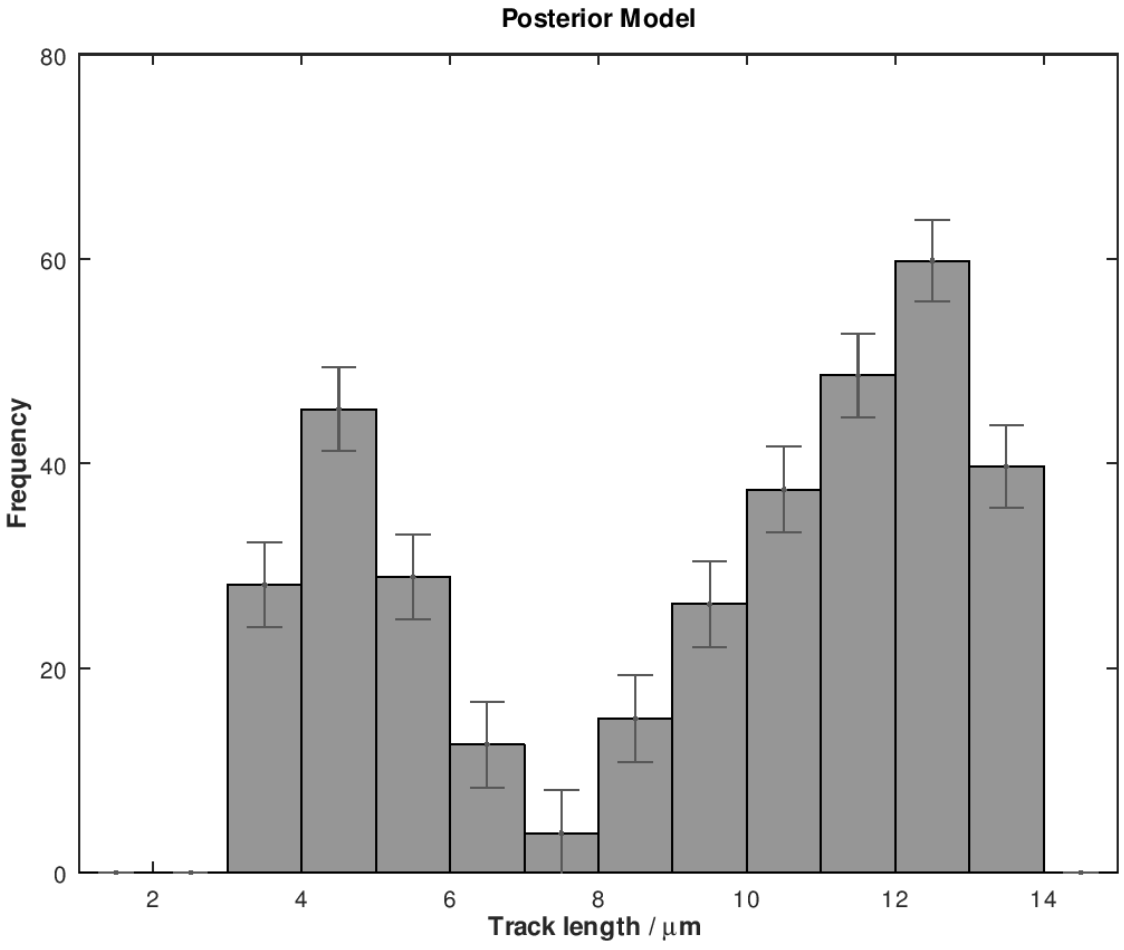

Figure D3: The corrected histogram as a result of the inversion of the 3D–histogram shown in Fig. D1.

410

The standard deviations are the diagonal values of the posterior covariance matrix. The result of the inversion is evaluated by comparing forward modeling using Eq. (21) with the inverted histogram as input data (Fig. D4). Compliance is good.

https://doi.org/10.5194/gchron-2021-8
Preprint. Discussion started: 2 March 2021

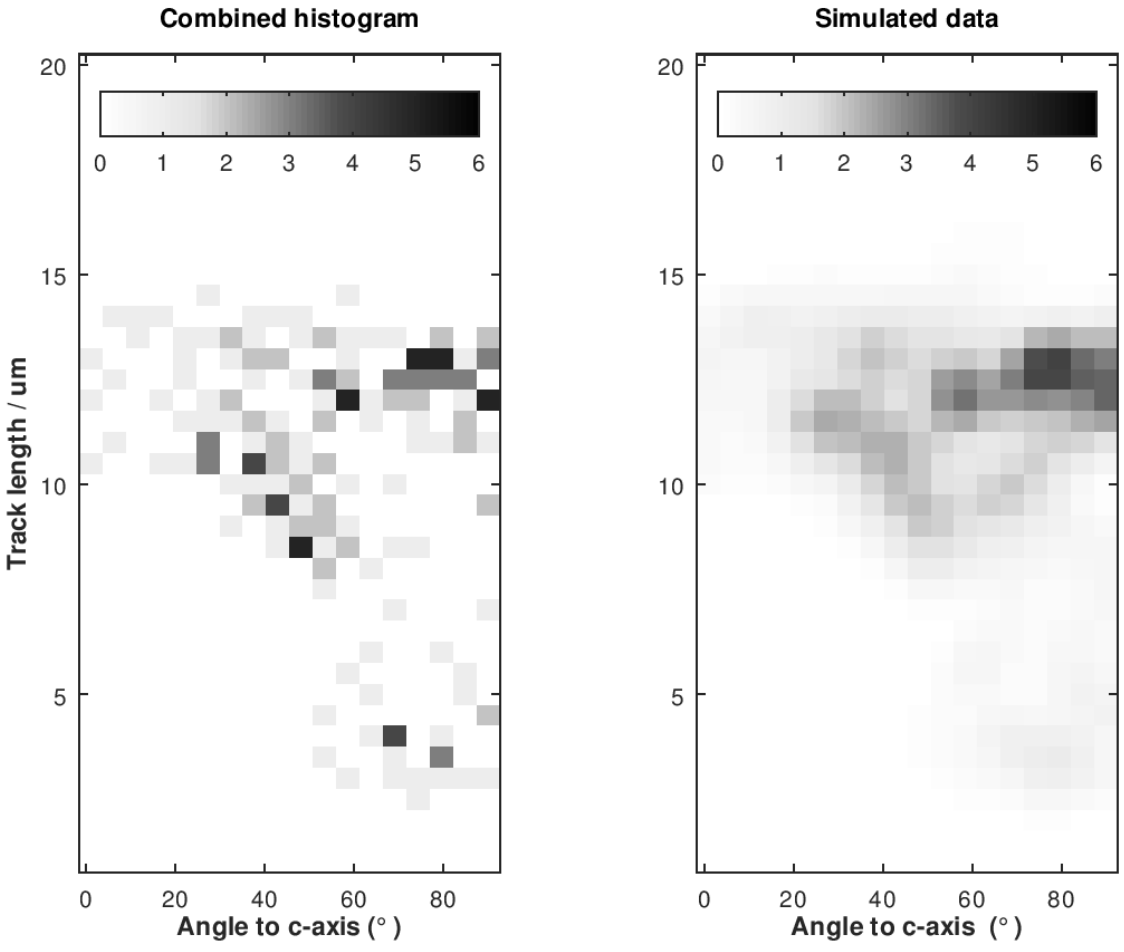

Figure D4: The combined 3D–histogram considered as synthetic data (Fig. D1) and the forwardly simulated approximation using the posterior model in Eq. (21). Grayscale is the number of tracks.

Code availability

Octave codes for reproducing the results shown in Fig. A1 and D1–4 are available online on Zenodo (https://doi.org/10.5281/zenodo.4553144; Jensen, 2021a) and (https://doi.org/10.5281/zenodo.4553291; Jensen, 2021b) for 2D– and 3D–histograms respectively.

https://doi.org/10.5194/gchron-2021-8
Preprint. Discussion started: 2 March 2021

Authors contribution

PJ developed the theory. During this process discussion with KH were important. PKJ wrote the equations, and the computer programmes. He also wrote the paper in tight dialog with KH. KH measured track lengths and surface track density used in the example shown in Fig. 4.

Competing interests

The authors declare that they have no conflict of interest.

References

Afra, B., Lang, M., Rodriguez, M. D., Zhang, J., Giulian, R., Kirby, N., Ewing, R. C., Trautmann, C., Toulemonde, M., and Kluth, P.: Annealing kinetics of latent particle tracks in Durango apatite, Phys. Rev. B, 83, 6, 064116, https://doi.org/10.1103/PhysRevB.83.064116, 2011.

Barbarand, J., Hurford, T., and Carter, A.: Variation in apatite fission-track length measurement: implications for thermal history modelling, Chem. Geol., 198, 1-2, 77-10, doi:10.1016/S0009-2541(02)00423-0, 2003.

Belton, D. X., and Raab, M. J.: Cretaceous reactivation and intensified erosion in the Archean–Proterozoic Limpopo Belt, demonstrated by apatite fission track thermochronology, Tectonophysics, 480, 1-4, 99-108, doi:10.1016/j.tecto.2009.09.018, 2010.

Bertagnolli, E., Keil, R., and Pahl, M.: Thermal history and length distribution of fission tracks in apatite, Part I., Nucl. Tracks Radiat. Meas. (1982), 7, 4, 163-177, doi:10.1016/0735-245X(83)90026-1, 1983.

Donelick, R. A., Ketcham, R. A., and Carlson, W. D.: Variability of apatite fission-track annealing kinetics: II. Crystallographic orientation effects, Am Min, 84, 9, 1224-1234, doi:10.2138/am-1999-0902, 1999.

Fleisher, R. L., Price, P. B., and Walker, R. M.: Nuclear Tracks in Solids: Principles and Applications, University of California Press, Berkeley, CA., 1975.

Galbraith, R. F.: Statistics for fission track analysis, Chapman and Hall/CRC, 165, 219, doi:10.1198/jasa.2007, 2005.

https://doi.org/10.5194/gchron-2021-8
Preprint. Discussion started: 2 March 2021

Gallagher, K.: Evolving temperature histories from apatite fission-track data, Earth Planet Sci Lett, 136, 3, 421-435, doi:10.1016/0012-821X(95)00197-K, 1995.

Gallagher, K.: Transdimensional inverse thermal history modeling for quantitative thermochronology, J. Geophys. Res. Solid Earth, 117, B2, http://doi.wiley.com/10.1029/2011JB008825, 2012.

Gleadow, A. J., Duddy, I. R., Green, P. F., and Hegarty, K. A.: Fission track lengths in the apatite annealing zone and the interpretation of mixed ages, Earth Planet Sci Lett, 78, 2-3, 245-254, doi:10.1016/0012-821X(86)90065-8, 1986a.

Gleadow, A. J. W., Duddy, I. R., Green, P. F., and Lovering, J. F.: Confined fission track lengths in apatite: a diagnostic tool for thermal history analysis, Contrib Mineral Petr, 94, 4, 405-415, doi:10.1007/BF00376334, 1986b.

Gleadow A., Kohn B., and Seiler C.: The Future of Fission-Track Thermochronology, in: Fission-Track Thermochronology and its Application to Geology, edited by Malusà M. and Fitzgerald P., Springer Textbooks in Earth Sciences, Geography and Environment, Springer, Cham, doi:10.1007/978-3-319-89421-8_4, 2019.

Green, P. F., Duddy, I. R., Gleadow, A. J. W., Tingate, P. R., and Laslett, G. M.: Thermal annealing of fission tracks in apatite: 1. A qualitative description, Chem. Geol.: Isotope Geoscience section, 59, 237-253, doi:10.1016/0168-9622(86)90074-6, 1986.

Green, P. F.: The relationship between track shortening and fission track age reduction in apatite: combined influences of inherent instability, annealing anisotropy, length bias and system calibration, Earth Planet Sci Lett, 89, 3-4, 335-352, doi:10.1016/0012-821X(88)90121-5, 1988.

Green, P. F., Duddy, I. R., Laslett, G. M., Hegarty, K. A., Gleadow, A. J. W., and Lovering, J. F,
Thermal annealing of fission tracks in apatite 4. Quantitative modelling techniques and extension to geological timescales, Chem. Geol.: Isotope Geoscience section, 79, 2, 155-182, https://doi.org/10.1016/0168-9622(89)90018-3, 1989.

Hansen, K.: Thermotectonic evolution of a rifted continental margin: fission track evidence from the Kangerlussuaq area, SE Greenland, Terra Nova, 8, 5, 458-469, http://doi.wiley.com/10.1111/j.1365-3121.1996.tb00771.x, 1996.

Hansen, K., Bergman, S. C., and Henk, B.: The Jameson Land basin (east Greenland): a fission track study of the tectonic and thermal evolution in the Cenozoic North Atlantic spreading regime, Tectonophysics, 331, 3, 307-339, doi:10.1016/S0040-1951(00)00285-7, 2001.

Jensen, P. K., Hansen, K., and Kunzendorf, H.: A numerical model for the thermal history of rocks based on confined horizontal fission tracks. International Journal of Radiation Applications and Instrumentation, Part D. Nucl. Tracks Radiat. Meas., 20, 2, 349-359, doi: 10.1016/1359-0189(92)90064-3, 1992.

Jensen, P. K., Bidstrup, T., Hansen, K., and Kunzendorf, H.: The Use of Fission Track Measurements in Basin Modeling, in: Computerized Basin Analysis, edited by: Harff. J. and Merriam, D. F., Springer US, doi:10.1007/978-1-4615-2826-5_7, 1993.

Jensen, P. K. and Hansen, K.: Identifying the post-sedimentary part of fission track length histograms with inherited tracks, Thermo 2018, 16th International Conference on Thermochronology, Quedlinburg, Germany; 16-21 September 2018, https://doi.org/10.1002/essoar.10500031.1, 2018.

Jensen, P.K.: Age versus length of horizontal fission tracks represented by 2D-Histograms, Zenodo, https://doi.org/10.5281/zenodo.4553144, 2021a.

Jensen, P.K.: Age versus length of horizontal fission tracks represented by 3D-Histograms, Zenodo, https://doi.org/10.5281/zenodo.4553291, 2021b.

Jungerman, J. and Wright, S. C.: Kinetic Energy Release in Fission of U238, U235, Th232, and Bi209 by High Energy Neutrons, Phys. Rev., 76, 1112-1116, doi:10.1103/PhysRev.76.1112 , 1949.

Keil, R., Pahl, M., and Bertagnolli, E.: Thermal history and length distribution of fission tracks: Part II, International Journal of Radiation Applications and Instrumentation, Part D. Nucl. Tracks Radiat. Meas., 13, 1, 25-33, 1987.

Ketcham, R. A.: Observations on the relationship between crystallographic orientation and biasing in apatite fission-track measurements, Am Min, 88, 5-6, 817-829, 2003.

Ketcham, R. A.: Forward and inverse modeling of low-temperature thermochronometry data, Rev Mineral and Geochem, 58, 1, 275-314, doi:10.2138/am-2003-5-610, 2005.

Ketcham, R. A., Donelick, R. A., Balestrieri, M. L., and Zattin, M.: Reproducibility of apatite fission-track length data and thermal history reconstruction, Earth Planet Sci Lett, 284, 3-4, 504-515, 2009.

https://doi.org/10.5194/gchron-2021-8
Preprint. Discussion started: 2 March 2021

Ketcham R.A.: Fission-Track Annealing: From Geologic Observations to Thermal History Modeling, in: Fission-Track Thermochronology and its Application to Geology, edited by: Malusà M. and Fitzgerald P, Springer Textbooks in Earth Sciences, Geography and Environment, Springer, Cham., https://doi.org/10.1007/978-3-319-89421-8_3, 2019.

Kirkpatrick, S., Gelatt, C. D., and Vecchi, M. P.: Optimization by simulated annealing, Science, 220, 4598, 671-680, 1983.

Laslett, G. M., Gleadow, A. J. W., and Duddy, I. R.: The relationship between fission track length and track density in apatite, Nucl. Tracks Radiat. Meas., (1982), 9, 1, 29-38, doi:10.1016/0735-245X(84)90019-X, 1984.

Li, W., Wang, L., Lang, M., Trautmann, C., and Ewing, R. C.: Thermal annealing mechanisms of latent fission tracks: Apatite vs. zircon, Earth Planet Sci Lett, 302, 1, 227-235, doi:10.1016/j.epsl.2010.12.016, 2011.

Lutz, T. M. and Omar, G.: An inverse method of modeling thermal histories from apatite fission-track data, Earth Planet Sci Lett, 104, 2-4, 181-195, doi:10.1016/0012-821X(91)90203-T 1991.

Tarantola, A.: Inverse problem theory, SIAM, Philadelphia, doi:0.1137/1.9780898717921, 2005.

Willett, S. D.: Inverse modeling of annealing of fission tracks in apatite; 1, A controlled random search method, Am. J. Sci., 297, 10, 939-969, doi:10.2475/ajs.297.10.939, 1997.